

# Cluster states and monopole transitions in $^{16}\text{O}$

Yoshiko Kanada-En'yo

*Department of Physics, Kyoto University, Kyoto 606-8502, Japan*

Cluster structures and monopole transitions in positive parity states of  $^{16}\text{O}$  were investigated based on the generator coordinate method calculation of an extended  $^{12}\text{C}+\alpha$  cluster model. The ground and excited states of a  $^{12}\text{C}$  cluster are taken into account by using  $^{12}\text{C}$  wave functions obtained with the method of antisymmetrized molecular dynamics. The  $0_2^+$  state of  $^{16}\text{O}$  and its rotational members, the  $2_1^+$  and  $4_1^+$  states are described well by the cluster states dominated by the  $^{12}\text{C}(0_1^+)+\alpha$  structure. Above the  $^{12}\text{C}(0_2^+)+\alpha$  threshold energy, we obtained a  $0^+$  state having the  $^{12}\text{C}(0_2^+)+\alpha$  cluster structure, which is considered to be a candidate for the  $4\alpha$  cluster gas state. The band structures were discussed based on the calculated  $E2$  transition strength. Isoscalar Monopole excitations from the ground state were also discussed.

## I. INTRODUCTION

Cluster structure is one of the essential features of nuclei as well as mean-field feature. Well developed cluster structures have been known, in particular, in excited states of stable light nuclei and also discovered in unstable nuclei. In these years, a new type of cluster state, a  $\alpha$  cluster gas state, has been suggested in light  $Z = N$  nuclei [1–7]. It has been proposed that  $2\alpha$  and  $3\alpha$  cluster gas states are realized in the  $0_1^+$  state of  $^8\text{Be}$  and the  $0_2^+$  state of  $^{12}\text{C}$ , where all  $\alpha$  clusters are almost freely moving in a dilute density like a gas. It is a challenging problem to search for such cluster gas states in other nuclei. For instance, possibility of  $\alpha$  cluster gas states in  $Z = N = 2n$  nuclei up to  $^{40}\text{Ca}$  was discussed in the systematic study with a non-microscopic cluster model, which suggested that  $\alpha$  cluster gases may appear in the energy region near the corresponding  $n$ - $\alpha$  break-up threshold consistently to the Ikeda threshold rule[3]. Cluster gas states including non- $\alpha$  clusters or those around a core nucleus were also suggested in excited states of  $^{11}\text{B}$ ,  $^8\text{He}$  and  $^{10}\text{Be}$ [8–14].

Recently, the search for  $4\alpha$  cluster gas state in excited states of  $^{16}\text{O}$  has been performed in experimental and theoretical works[5, 6, 15]. The semi-microscopic  $4\alpha$  calculation by Funaki *et al.* suggested that the  $^{16}\text{O}(0_6^+)$  state near the  $4\alpha$  threshold has the large  $^{12}\text{C}(0_2^+)+\alpha$  component and is a candidate for the dilute  $4\alpha$  cluster gas state [5, 6]. It is also an interesting problem to assign band members of the cluster gas state to clarify the property of the cluster gas, especially, stability against rotation as discussed in Refs. [16, 17].

$^{16}\text{O}$  is a double closed-shell nuclei and its ground state is dominated by  $p$ -shell closed configuration, while there exist many excited states that are difficult to be described by a simple shell model. Semi-microscopic and microscopic  $^{12}\text{C}+\alpha$  cluster models [18–20] were applied to study excited states of  $^{16}\text{O}$  and it has been shown that many excited states can be described by  $^{12}\text{C}+\alpha$  cluster structures. For instance, in the calculation with the  $^{12}\text{C}+\alpha$  orthogonality condition model (OCM) [18], a semi-microscopic cluster model [21], the  $0_2^+$  state of  $^{16}\text{O}$  and its rotational band members, the  $2_1^+$  and  $4_1^+$  states, are described by the cluster state having the dom-

inant  $^{12}\text{C}(0_1^+)+\alpha$  component. Moreover, the  $^{16}\text{O}(0_3^+)$  state is considered to mainly have the  $^{12}\text{C}(2_1^+)+\alpha$  component. These results are supported also by  $4\alpha$ -OCM calculations [5, 6, 22]. Thus, many excited states up to  $\sim 14$  MeV are considered to be weak-coupling  $^{12}\text{C}+\alpha$  cluster states having large components of  $^{12}\text{C}(0_1^+)+\alpha$ ,  $^{12}\text{C}(2_1^+)+\alpha$ , and so on. The cluster structures of these excited states are supported by the experimental data of  $E2$  and monopole transition strengths as well as the  $\alpha$ -decay widths [18, 19, 23].

Above these  $^{12}\text{C}+\alpha$  cluster states, a  $4\alpha$  cluster state was predicted at the energy near the  $4\alpha$  and  $^{12}\text{C}(0_2^+)+\alpha$  threshold energies by Funaki *et al.* with the  $4\alpha$ -OCM [5, 6]. This state has the large  $^{12}\text{C}(0_2^+)+\alpha$  component, that is, the  $3\alpha$  cluster gas state of the  $^{12}\text{C}(0_2^+)$  with an additional  $\alpha$  around the  $3\alpha$  gas. The large occupation probability of 4  $\alpha$  particles in the same  $0S$  and low-momentum orbit was demonstrated by the analysis of the  $4\alpha$ -OCM wave function.

In spite of the success of those calculations with the semi-microscopic cluster models such as the  $^{12}\text{C}+\alpha$ -OCM and the  $4\alpha$ -OCM, there is no microscopic calculation that can reproduce the excitation energies of the cluster states in  $^{16}\text{O}$ . The microscopic calculations with the resonating group method (RGM)[24] and the generator coordinate method (GCM)[25] of  $^{12}\text{C}+\alpha$  cluster models[19, 20] failed to reproduce the experimental excitation energy of the  $0_2^+$  at 6.05 MeV. They largely overestimated it by a factor 2–3 as  $E_x(0_2^+) \sim 16$  MeV. One of the most crucial problems in microscopic calculations using effective nuclear forces for  $^{16}\text{O}$  is the underbinding problem of  $^{12}\text{C}$  relative to  $^{16}\text{O}$ , or in other words, the overbinding problem of  $^{16}\text{O}$  relative to  $^{12}\text{C}$ .

Our aim is to investigate cluster structures of excited states of  $^{16}\text{O}$ . In particular, we search for a highly excited  $0^+$  state having the  $^{12}\text{C}(0_2^+)+\alpha$  structure, which may be the candidate for the  $4\alpha$  gas state. We perform the GCM calculation of an extended  $^{12}\text{C}+\alpha$  model. In the present calculation, we adopt the  $^{12}\text{C}$  wave functions obtained with the variation after the parity and angular-momentum projections(VAP) in the framework of antisymmetrized molecular dynamics (AMD) [26, 27]. As shown in the previous works on  $^{12}\text{C}$  [28, 29], the

AMD+VAP calculation succeeded to describe well the structures of ground and excited states of  $^{12}\text{C}$ , such as the developed  $3\alpha$ -cluster structure in the excited states as well as the ground state properties. The binding energy of  $^{12}\text{C}$  was improved because of the energy gain of the spin-orbit force due to the mixing of  $p_{3/2}$ -shell configurations. We use the same effective nuclear force used in the previous study of  $^{12}\text{C}$ , that is, the MV1 force [30] containing the phenomenological three-body repulsive force to avoid the overshooting problem of the binding energy in heavier nuclei. To take into account the ground and excited states of  $^{12}\text{C}$  we superpose the  $^{12}\text{C}$  AMD wave functions and approximately perform the double projection, that is the angular-momentum projection of the subsystem  $^{12}\text{C}$  and that of the total system. Isoscalar monopole excitations in  $^{16}\text{O}$  are also discussed.

This paper is organized as follows. In the next section, we explain the formulation of the present calculation. The results are shown in III, and isoscalar monopole excitations are discussed in IV. Finally, a summary and outlooks are given in V.

## II. FORMULATION

### A. $^{12}\text{C}(\text{AMD})+\alpha\text{GCM}$ calculation for $^{16}\text{O}$

The ground and excited states of  $^{16}\text{O}$  are described by using an extended  $^{12}\text{C}+\alpha$  cluster wave function. To describe inter-cluster motion, the distance  $d$  between the mean positions of  $^{12}\text{C}$  and  $\alpha$  centers is treated as the generator coordinate, and the  $^{12}\text{C}+\alpha$  wave functions with different  $d$  values are superposed. The  $\alpha$  cluster is written by the  $(0s)^4$  harmonic oscillator wave function  $\Phi_\alpha(3\mathbf{S}/4)$  which is localized around the position  $3\mathbf{S}/4$  with  $\mathbf{S} = (0, 0, d)$ . The  $^{12}\text{C}$  cluster is localized around  $-\mathbf{S}/4$  and described by the superposition of AMD wave functions.

An AMD wave function for the  $^{12}\text{C}$  cluster localized around the origin is given as follows,

$$\Phi_{^{12}\text{C}}^{\text{AMD}}(\mathbf{Z}) = \frac{1}{\sqrt{A_C!}} \mathcal{A}_C \{\varphi_1, \varphi_2, \dots, \varphi_{A_C}\}, \quad (1)$$

$$\varphi_i = \phi_{\mathbf{x}_i} \chi_i \tau_i, \quad (2)$$

$$\phi_{\mathbf{x}_i}(\mathbf{r}_j) = \left(\frac{2\nu}{\pi}\right)^{4/3} \exp\left\{-\nu\left(\mathbf{r}_j - \frac{\mathbf{x}_i}{\sqrt{\nu}}\right)^2\right\}, \quad (3)$$

$$\chi_i = \left(\frac{1}{2} + \xi_i\right)\chi_\uparrow + \left(\frac{1}{2} - \xi_i\right)\chi_\downarrow. \quad (4)$$

Here  $A_C$  is the mass number of  $^{12}\text{C}$ ,  $A_C = 12$ , and the operator  $\mathcal{A}_C$  is the antisymmetrizer of the  $A_C$  nucleons. The wave function  $\Phi_{^{12}\text{C}}^{\text{AMD}}(\mathbf{Z})$  is written by a Slater determinant of single-particle wave functions  $\varphi_i$ , each of which is given by a product of the spatial ( $\phi_{\mathbf{x}_i}$ ), the intrinsic spin ( $\chi_i$ ), and isospin ( $\tau_i$ ) functions. The isospin function fixed to be up (proton) or down (neutron). The spatial part  $\phi_{\mathbf{x}_i}$  is written by the Gaussian wave packet localized around the position  $\mathbf{x}_i$  in

the phase space. Accordingly, an AMD wave function is expressed by a set of variational parameters,  $\mathbf{Z} \equiv \{\mathbf{X}_1, \mathbf{X}_2, \dots, \mathbf{X}_{A_C}, \xi_1, \xi_2, \dots, \xi_{A_C}\}$ , which expresses an AMD configuration of the  $^{12}\text{C}$  cluster. The mean position  $\{\mathbf{X}_1 + \mathbf{X}_2 + \dots + \mathbf{X}_{A_C}\}/A_C$  of  $^{12}\text{C}$  mass center is set on the origin.

The  $^{12}\text{C}$  wave function is shifted from the origin to the position  $-\mathbf{S}/4$  by shifting the Gaussian center parameters  $\mathbf{x}_i \rightarrow \mathbf{x}_i - \mathbf{S}/4$ . The shifted  $^{12}\text{C}$  AMD wave function is denoted by  $\Phi_{^{12}\text{C}}^{\text{AMD}}(-\mathbf{S}/4; \mathbf{Z})$ . An wave function  $\Phi_{^{12}\text{C}}^{\text{AMD}}(-\mathbf{S}/4; \mathbf{Z})$  corresponds to the  $^{12}\text{C}$  cluster around  $-\mathbf{S}/4$  having an intrinsic wave function specified by the set of parameters  $\mathbf{Z}$ . To construct the angular-momentum eigen state of the subsystem  $^{12}\text{C}$  projected from the intrinsic state, it is necessary to superpose rotated states of the intrinsic wave function. For an configuration  $\mathbf{Z} = \mathbf{Z}^{(k)}$  ( $k$  is the label for the configuration) of the  $^{12}\text{C}$  AMD wave function, we prepare rotated states  $R^{\text{sub}}(\Omega')\Phi_{^{12}\text{C}}^{\text{AMD}}(-\mathbf{S}/4; \mathbf{Z}^{(k)})$  of the subsystem  $^{12}\text{C}$ . Here  $R^{\text{sub}}(\Omega')$  is the operator of the Euler angle  $\Omega'$  rotation of the subsystem around  $-\mathbf{S}/4$ . A wave function of  $^{16}\text{O}$  is given by performing the antisymmetrization of all nucleons and the parity and angular-momentum projections,

$$\Phi_{^{12}\text{C}+\alpha}^{J\pi K}(d, \Omega'_j, \mathbf{Z}^{(k)}) = P_{MK}^{J\pi} \mathcal{A} \left\{ R^{\text{sub}}(\Omega') \Phi_{^{12}\text{C}}^{\text{AMD}}(-\mathbf{S}/4; \mathbf{Z}^{(k)}) \cdot \Phi_\alpha(3\mathbf{S}/4) \right\} \quad (5)$$

Here  $\mathcal{A}$  is the antisymmetrizer for all sixteen nucleons and  $P_{MK}^{J\pi}$  is the parity ( $\pi$ ) and angular-momentum projection operator for the total system.

We superpose  $^{16}\text{O}$  wave functions constructed from the  $^{12}\text{C}$  AMD wave function and the  $\alpha$  cluster wave function. Each  $^{16}\text{O}$  wave function is specified by the AMD configuration  $\mathbf{Z}^{(k)}$ , the rotation angle  $\Omega'_j$  for the  $^{12}\text{C}$  cluster, and the inter-cluster distance  $d_i$ . Then the final  $^{16}\text{O}$  wave function in the present  $^{12}\text{C}(\text{AMD})+\alpha\text{GCM}$  model is written as follows,

$$\Psi_{\text{AMD}+\alpha\text{GCM}}^{J_n^\pi} = \sum_{K,i,j,k} c^{J_n^\pi}(K, i, j, k) \Phi_{^{12}\text{C}+\alpha}^{J\pi K}(d_i, \Omega'_j, \mathbf{Z}^{(k)}). \quad (6)$$

The coefficients  $c^{J_n^\pi}(K, i, j, k)$  for the  $J_n^\pi$  state are treated as independent parameters and they are determined by solving the Hill-Wheeler equation as done in the GCM[25]. In principle, the superposition of rotated states of the  $^{12}\text{C}$  cluster is equivalent to the so-called "double projection", in which the angular-momentum projections are done for the subsystem  $^{12}\text{C}$  and also for the total system. It corresponds to take into account different spin states of the  $^{12}\text{C}$  cluster. In the practical calculation, however, we use only a limited number of the rotation angle  $\Omega'_j$  and it is an approximated method of the double projection. By superposing several AMD configurations of  $^{12}\text{C}$ , excited states as well as the ground state of the  $^{12}\text{C}$  cluster are incorporated. The details of the AMD configurations of  $^{12}\text{C}$  are explained later.

For general nuclei, we can consider the extended cluster model "AMD+ $\alpha$ GCM", in which a core nucleus is

written by AMD wave functions and relative motion between an  $\alpha$  cluster and the core is taken into account by superposing core- $\alpha$  cluster wave functions with various values of the distance  $d$ . Based on a similar concept, core+ $n$  cluster models have been already used to describe a valence neutron motion around the core expressed by AMD wave functions in the studies of neutron-rich nuclei. Firstly a  $^{10}\text{Be}(\text{AMD})+n\text{GCM}$  model without the angular-momentum projection of subsystem has been adopted to  $^{11}\text{Be}$ [26], and recently,  $^{30}\text{Ne}(\text{AMD})+n\text{GCM}$  and  $^{12}\text{Be}(\text{AMD})+n\text{GCM}$  models have been applied to  $^{31}\text{Ne}$  and  $^{13}\text{Be}$  [31, 32].

## B. Wave functions of $^{12}\text{C}$

In the previous work on  $^{12}\text{C}$ [28, 29], the AMD+VAP method has been applied to  $^{12}\text{C}$  and it has been proved to describe well the structures of the ground and excited states in  $^{12}\text{C}$ . To describe the  $^{12}\text{C}$  cluster in the present  $^{12}\text{C}(\text{AMD})+\alpha\text{GCM}$  calculation, we use the intrinsic wave functions of  $^{12}\text{C}$  obtained with the AMD+VAP in Ref. [29].

We here briefly explain the AMD+VAP method[28, 29]. More details of the method are described in Ref. [29]. As mentioned before, the AMD wave function of  $^{12}\text{C}$  explained in Eq. 1 is specified by the set of parameters,  $\mathbf{Z} = \{\mathbf{X}_1, \mathbf{X}_2, \dots, \mathbf{X}_{A_C}, \xi_1, \xi_2, \dots, \xi_{A_C}\}$ . In the AMD framework, these are treated as variational parameters and determined by the energy variation. In the AMD+VAP method, the energy variation is performed after the spin-parity projection. Namely, the parameters  $\mathbf{X}_i$  and  $\xi_i (i = 1 \sim A)$  are varied to minimize the energy expectation value of the Hamiltonian,  $\langle \Phi | H | \Phi \rangle / \langle \Phi | \Phi \rangle$ , with respect to the spin-parity eigen wave function  $\Phi = P_{MK}^{J\pi} \Phi_{12\text{C}}^{\text{AMD}}(\mathbf{Z})$  projected from the AMD wave function of  $^{12}\text{C}$ . Then the optimum AMD wave function  $\Phi_{12\text{C}}^{\text{AMD}}(\mathbf{Z}^{J\pi})$ , which approximately describes the intrinsic wave function for the  $J_1^\pi$  state, is obtained. For higher  $J_n^\pi$  states, the variation is done for the component orthogonal to the lower  $J^\pi$  states. For each  $J(k)_{n(k)}^{\pi(k)}$ , the optimum parameters  $\mathbf{Z}^{(k)}$  are obtained. Here  $(k)$  is the label for the AMD configuration for the  $J(k)_{n(k)}^{\pi(k)}$  state. After the VAP procedure, final wave functions for  $J^\pi$  states are expressed by the superposition of the spin-parity eigen wave functions projected from all the intrinsic wave functions  $\Phi_{12\text{C}}^{\text{AMD}}(\mathbf{Z}^{(k)})$  as,

$$\Psi_{12\text{C}}^{J_n, \pi} = \sum_{K, k} c_{12\text{C}}^{J_n, \pi}(K, k) |P_{MK}^{J_n, \pi} \Phi_{12\text{C}}^{\text{AMD}}(\mathbf{Z}^{(k)})|, \quad (7)$$

where the coefficients  $c_{12\text{C}}^{J_n, \pi}(K, k)$  are determined by solving the Hill-Wheeler equation, i.e., the diagonalization of the norm and Hamiltonian matrices.

In the previous study of  $^{12}\text{C}$ , totally, 23 AMD configurations  $\Phi_{12\text{C}}^{\text{AMD}}(\mathbf{Z}^{(k)})$  ( $k = 1, \dots, 23$ ) are obtained by the energy variation for  $J(k)_{n(k)}^{\pi(k)} =$

$0_1^+, 0_2^+, 0_3^+, 1_1^+, 2_1^+, 2_2^+, 2_3^+, \dots, 1_1^-, 2_1^-, 3_1^-, \dots$ , and they are adopted as basis wave functions of the final wave functions of  $^{12}\text{C}$ . In the present  $^{12}\text{C}(\text{AMD})+\alpha\text{GCM}$  calculation, we adopt only three basis wave functions to save the computational cost. In order to take into account the ground and second  $0^+$  states of  $^{12}\text{C}$ , we choose two basis wave functions of  $J(k)_{n(k)}^{\pi(k)} = 0_1^+, 0_2^+$  for  $k = 1, 2$ . We also adopt the basis wave function of  $J(k)_{n(k)}^{\pi(k)} = 1_1^-$  for  $k = 3$ . The intrinsic density of these three basis wave functions are shown in Fig. 1. The ground state has the compact structure of  $3\alpha$  with a mixing of the  $p_{3/2}$ -shell closure component, while the  $0_2^+$  and  $1_1^-$  states show developed  $3\alpha$  cluster structures.

The energy levels of  $^{12}\text{C}$  obtained with the truncated model space of three bases are shown in Fig. 2 compared with those with full 23 basis wave functions and experimental ones. With the truncation, we get reasonable reproduction of the energy levels of many positive and negative parity states though the full 23 basis wave functions gives better results, in particular, for excited states. The reason for  $\sim 2$  MeV higher energies of the  $0_2^+$  and  $1_1^-$  states with the three bases than those with the full bases is that these states gain their energy by the superposition of various configurations of the  $3\alpha$  cluster.

We also calculate the overlap  $\mathcal{N}(^{16}\text{O}(J_n^\pi); ^{12}\text{C}(0_n^+) + \alpha; d)$  of the  $^{16}\text{O}$  wave function obtained by the  $^{12}\text{C}(\text{AMD})+\alpha\text{GCM}$  and the  $^{12}\text{C}(0_n^+) + \alpha$  wave function having a certain distance  $d$ ,

$$\begin{aligned} \Phi_{12\text{C}(0_n^+) + \alpha}^{J_n, \pi}(d) &\equiv n_0 P_{00}^{J_n, \pi} \mathcal{A} \{ \\ &\sum_k c_{12\text{C}}^{0_n^+}(K=0, k) P_{00}^{J_n, \pi} \Phi_{12\text{C}}^{\text{AMD}}(-\mathbf{S}/4; \mathbf{Z}^{(k)}) \\ &\times \Phi_\alpha(3\mathbf{S}/4) \}, \end{aligned} \quad (8)$$

$$\begin{aligned} \mathcal{N}(^{16}\text{O}(J_n^\pi); ^{12}\text{C}(0_n^+) + \alpha; d) \\ &\equiv |\langle \Psi_{\text{AMD}+\alpha\text{GCM}}^{J_n, \pi} | \Phi_{12\text{C}(0_n^+) + \alpha}^{J_n, \pi}(d) \rangle|^2. \end{aligned} \quad (9)$$

Here  $n_0$  is the normalization factor to satisfy

$$|\langle \Phi_{12\text{C}(0_n^+) + \alpha}^{J_n, \pi}(d) | \Phi_{12\text{C}(0_n^+) + \alpha}^{J_n, \pi}(d) \rangle|^2 = 1, \quad (10)$$

and the  $\Omega'$  integration in the operator  $P_{00}^{J_n, \pi}$  of the  $J=0$  angular-momentum projection of the subsystem is approximated by the sum of the finite number mesh points,  $P_{00}^{J_n, \pi} = \sum_j R^{\text{sub}}(\Omega'_j)$ . In the present work, we calculate the overlap only with the  $^{12}\text{C}(0_n^+)$ -cluster wave function because of the approximation with the finite points of the Euler angle  $\Omega'_j$  for the rotation of subsystem  $^{12}\text{C}$ .

## C. Parameters in numerical calculations

The width parameter  $\nu$  of the  $^{12}\text{C}$  cluster is  $\nu = 0.19 \text{ fm}^{-2}$  which was used in the previous work on  $^{12}\text{C}$  in Ref. [29]. The width parameter of the  $\alpha$  cluster is taken to be the same value  $\nu = 0.19 \text{ fm}^{-2}$  because the center of

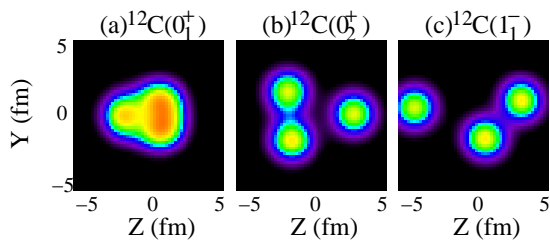


FIG. 1: (Color online) Density distribution of the intrinsic states of (a)  $^{12}\text{C}(0_1^+)$ , (b)  $^{12}\text{C}(0_2^+)$ , and (c)  $^{12}\text{C}(1_1^-)$  calculated with the AMD+VAP [29]. The orientation of an intrinsic state is chosen so as to satisfy  $\langle x^2 \rangle \leq \langle y^2 \rangle \leq \langle z^2 \rangle$  and  $\langle xy \rangle = \langle yz \rangle = \langle zx \rangle = 0$ . The horizontal and vertical axes are set to the  $z$  and  $y$  axes, respectively. Densities are integrated with respect to the  $x$  axis.

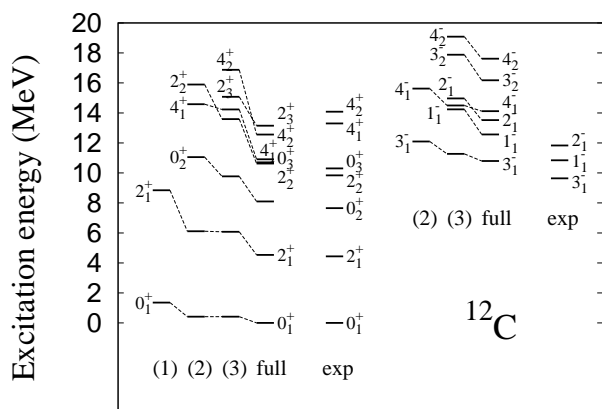


FIG. 2: Energy spectra of  $^{12}\text{C}$  calculated with the AMD+VAP using three basis AMD wave functions  $\Phi_{^{12}\text{C}}^{\text{AMD}}(\mathbf{Z}^{(k)})$  obtained by the energy variation for  $J(k)_n^{(k)\pi} = 0_1^+, 0_2^+$  and  $1_1^-$  with  $k = 1, 2$  and  $3$ , respectively, and that using the full 23 basis AMD wave functions. The  $0_1^+$  energy calculated with the 23 bases is adjusted to 0 and the relative energies are plotted. The energies calculated using (1) one basis ( $k = 1$ ), (2) two bases ( $k = 1, 2$ ), (3) three bases ( $k = 1, 2, 3$ ), and (full) the full bases are shown. The excitation energies of the experimental data are also shown.

mass motion can be exactly extracted when a common width parameter is used for all clusters.

For the inter-cluster distance between  $^{12}\text{C}$  and  $\alpha$ , six points  $d_i = 1.2, 2.4, 3.6, \dots, 7.2$  fm are chosen. The choice of  $d_i \leq 7.2$  fm corresponds to a kind of bound state approximation. In the angular-momentum projection of the total system, the integration of the Euler angle  $\Omega = (\theta_1, \theta_2, \theta_3)$  is numerically performed by the summation of mesh points (23, 46, 23) of the angles  $(\theta_1, \theta_2, \theta_3)$ .

For the intrinsic states of  $^{12}\text{C}$  labeled by  $(k)$ , three AMD configurations are adopted. For each intrinsic state  $(k)$  at the distance  $d_i$ , seventeen rotated states  $R^{\text{sub}}(\Omega'_j)\Phi_{^{12}\text{C}}^{\text{AMD}}(-\mathbf{S}/4; \mathbf{Z}^{(k)})$  ( $j = 1, \dots, 17$ ) are constructed. The Euler angle  $\Omega' = (\theta'_1, \theta'_2, \theta'_3)$  are

chosen to be  $\theta'_1 = (0, \pi/4, \pi/2, 3\pi/4, \pi)$  and  $\theta'_2 = (0, \pi/4, \pi/2, 3\pi/4, \pi)$ . We omit the points  $\theta'_2 = (5\pi/4, 3\pi/2, 7\pi/4)$  in the region  $\pi < \theta'_2 < 2\pi$  to save the numerical cost. This is valid when the intrinsic state has the symmetry such as an isosceles triangle  $3\alpha$  configuration.  $\theta'_3$  is fixed to be  $\theta'_3 = 0$  because the rotation  $\theta'_3$  is effectively done by the  $K$  projection in the angular-momentum projection of the total system because of the rotational invariance of the  $\alpha$  cluster. As for the  $K$ -mixing, we truncate the  $|K| \geq 4$  components.

### III. RESULTS

#### A. Effective nuclear interaction

In the present calculation of the  $^{12}\text{C}(\text{AMD})+\alpha\text{GCM}$ , we use the same effective nuclear interaction with the same parameters as those used in the previous calculation of  $^{12}\text{C}$ [29]. It is the MV1 force [30] for the central force supplemented by the two-body spin-orbit force with the two-range Gaussian form same as that in the G3RS force [33]. The Coulomb force is approximated using a seven-range Gaussian form. The Majorana, Bartlett, and Heisenberg parameters in the MV1 force are  $m = 0.62$ ,  $b = 0$ , and  $h = 0$ , respectively, and the spin-orbit strengths are taken to be  $u_I = -u_{II} = 3000$  MeV.

#### B. Energy levels of $0^+$ states

In the preceding studies[5, 6, 18–20, 22], developed cluster structures were suggested in excited  $0^+$  states of  $^{16}\text{O}$ . It is considered that the ground state of  $0_1^+$  is dominated by the doubly closed-shell structure, while the  $0_2^+$  state has the  $^{12}\text{C}(0_1^+)+\alpha$  structure. The  $0_3^+$  state is suggested to have the  $^{12}\text{C}(2_1^+)+\alpha$  component. In the  $4\alpha$ -OCM calculation, it was suggested that the  $0_4^+$  mainly has the  $^{12}\text{C}(0_1^+)+\alpha$  structure with higher nodal behavior of  $\alpha$  cluster around  $^{12}\text{C}$  and the  $0_5^+$  contains the  $^{12}\text{C}(1_1^-)+\alpha$  component. In the study with the  $4\alpha$ -OCM calculation by Funaki *et al.*[5, 6], the  $0_6^+$  state having the  $^{12}\text{C}(0_2^+)+\alpha$  structure was suggested and regarded as the  $4\alpha$  cluster gas state. They proposed that the experimental  $0_6^+$  state at 15.1 MeV is a candidate for the  $4\alpha$  cluster gas state.

The energy levels of  $0^+$  states of  $^{16}\text{O}$  up to the fifth  $0^+$  state calculated with the  $^{12}\text{C}(\text{AMD})+\alpha\text{GCM}$  calculation are shown in Fig. 3 compared with the experimental data. The theoretical energy levels with other theoretical calculations,  $4\alpha$ -OCM[5, 6] and  $^{12}\text{C}+\alpha$ -OCM[18], are also shown.

In the present result, the ground state ( $0_1^+$ ) has mainly the doubly closed-shell structure with less development of cluster, while the second  $0^+$  state ( $0_{II}^+$ ) is described mainly by the developed  $^{12}\text{C}(0_1^+)+\alpha$  structure. The cluster structure of the  $0_{II}^+$  state is consistent with that of

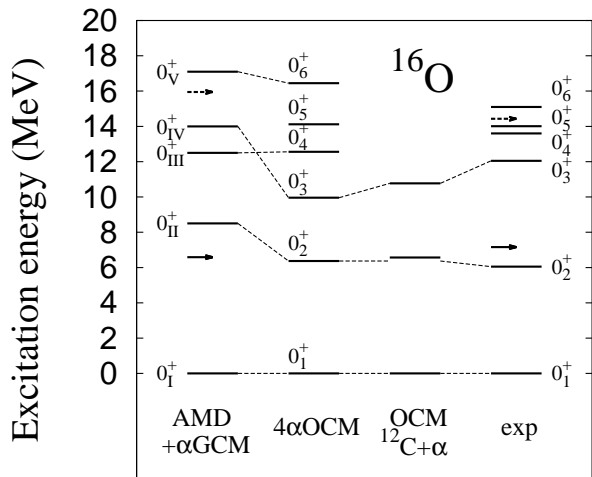


FIG. 3: Excitation energies of  $0^+$  states in  $^{16}\text{O}$  calculated with the present  $^{12}\text{C}(\text{AMD})+\alpha\text{GCM}$  (AMD+ $\alpha\text{GCM}$ ) and those of the  $4\alpha\text{-OCM}$  and  $^{12}\text{C}+\alpha\text{-OCM}$  from Refs. [5, 18]. The experimental energy levels of  $0^+$  states are taken from Refs. [15, 34]. The  $^{12}\text{C}(0_1^+)+\alpha$  and  $^{12}\text{C}(0_2^+)+\alpha$  threshold energies are plotted by solid and dashed arrows, respectively.

the preceding works and can be assigned to the experimental  $0_2^+$  state at 6.05 MeV. Above the second  $0^+$  state, we obtain the third  $0^+$  state ( $0_{III}^+$ ) having further developed  $^{12}\text{C}(0_1^+)+\alpha$  structure and the fourth  $0^+$  state ( $0_{IV}^+$ ) showing a feature of the  $^{12}\text{C}(2_1^+)+\alpha$  structure. The features of the  $0_{III}^+$  and  $0_{IV}^+$  states are consistent with the  $0_4^+$  and  $0_3^+$  states in the  $4\alpha\text{-OCM}$  calculation [5, 6, 23], respectively. The ordering of the  $0_{III}^+$  and  $0_{IV}^+$  is opposite to that of the  $4\alpha\text{-OCM}$  calculation. If we assign the  $0_{IV}^+$  state to the  $0_3^+$  at 12.05 MeV, the experimental level spacing between the  $0_2^+$  and  $0_3^+$  state is reproduced well by the present calculation. For the  $0_{III}^+$  state, the dominant  $^{12}\text{C}(0_1^+)+\alpha$  structure with an  $\alpha$  far from the  $^{12}\text{C}(0_1^+)$  core is consistent with the  $0_4^+$  state in the  $4\alpha\text{-OCM}$  calculation which is assigned to the  $0_4^+$  state at 13.6 MeV from its relatively large width. The present calculation is a bound state approximation, and therefore it is difficult to discuss the width. Moreover, stability of this state should be checked carefully by taking into account mixing of continuum states.

In the present calculation, we obtain the fifth  $0^+$  state ( $0_V^+$ ) having the developed  $^{12}\text{C}(0_2^+)+\alpha$  structure. As discussed later, it has a large  $^{12}\text{C}(0_2^+)+\alpha$  component with an  $\alpha$  cluster moving around the  $^{12}\text{C}(0_2^+)$  cluster in the  $S$ -wave channel and it is consistent with the structure of the  $4\alpha$  cluster gas state in the  $0_6^+$  suggested by the  $4\alpha\text{-OCM}$  calculation. The  $0_V^+$  state has a significant  $\alpha$ -cluster amplitude about 4 ~ 5 fm far from the  $^{12}\text{C}(0_2^+)$  core. This is the same region of the  $\alpha$ -cluster amplitude in the  $^{12}\text{C}(0_2^+)$ . Considering that the  $^{12}\text{C}(0_2^+)$  has the  $3\alpha$  cluster gas feature and the fourth  $\alpha$  is moving in  $S$ -wave

in the same region of  $3\alpha$  clusters, the  $0_V^+$  state can be regarded as a  $4\alpha$  cluster gas state similar to the  $3\alpha$  cluster gas in the  $^{12}\text{C}(0_2^+)$ .

TABLE I: The charge radii( $R_c$ ),  $E0$  transition matrix elements( $M(E0)$ ), and the ratio( $P_{E.w.}$ ) to the EWSR of the isoscalar  $E0$  transition that is 1/4 of the isoscalar monopole EWSR. The theoretical values are those calculated with the present  $^{12}\text{C}(\text{AMD})+\alpha\text{GCM}$ , the  $4\alpha\text{-OCM}$ [23], the  $^{12}\text{C}+\alpha\text{-OCM}$ [18]. The charge radius of a proton 0.887 fm [35] is used to evaluate the charge radii of  $0^+$  states in  $^{16}\text{O}$ . Experimental data are taken from Refs. [34–36].

state	$E_x$ (MeV)	$R_c$ (fm)	$M(E0)$	$P_{E.w.}$ (%)
$^{12}\text{C}(\text{AMD})+\alpha\text{GCM}$				
$0_1^+$	0.0	2.9		
$0_{II}^+$	8.5	3.5	4.0	5.4%
$0_{III}^+$	12.5	3.9	3.5	6.4%
$0_{IV}^+$	14.0	3.5	6.0	20%
$0_V^+$	17.1	3.8	1.4	1.4%
exp.				
$0_1^+$	0	2.70		
$0_2^+$	6.05		3.55(0.21)	3.5%
$0_3^+$	12.05		4.03(0.09)	9.1%
$0_4^+$	13.6			
$0_5^+$	14.01		3.3(0.7)	6.3%
$0_6^+$	15.1			
$4\alpha\text{-OCM}$				
$0_1^+$	0	2.7		
$0_2^+$	6.37	3	3.9	4%
$0_3^+$	9.96	3.1	3.9	6.3%
$0_4^+$	12.56	4	2.4	3%
$0_5^+$	14.12	3.1	2.6	3.9%
$0_6^+$	16.45	5.6	1.0	0.7%
$^{12}\text{C}+\alpha\text{-OCM}$				
$0_1^+$	0	2.5		
$0_2^+$	6.57	2.9	3.88	4.8%
$0_3^+$	10.77	2.8	3.5	6.4%

The root-mean-square charge radii and monopole transition matrices  $M(E0)$  for the  $0^+$  states are shown in Table I. The excited states tend to have large r.m.s. charge radii due to developed cluster structures compared with that of the ground state. In particular, the  $0_{III}^+$  state with the higher nodal  $^{12}\text{C}(0_1^+)+\alpha$  structure and  $0_V^+$  state with the  $^{12}\text{C}(0_2^+)+\alpha$  structure have about 1 fm larger radii than the ground state. The radii of the  $0_V^+$  state is smaller than the  $0_6^+$  state of the  $4\alpha\text{-OCM}$  calculation. It may come from the smaller radius of  $^{12}\text{C}(0_2^+)$  with the 3-basis AMD+VAP calculation than that with the  $3\alpha\text{-OCM}$  calculation[37]. Namely, the r.m.s. matter radius of  $^{12}\text{C}(0_2^+)$  is 3.2 fm in the 3-basis AMD+VAP result (3.3 fm in the full 23-basis AMD+VAP) and 4.31 fm in the  $3\alpha\text{-OCM}$  calculation.

Those excited states with developed cluster structures also have significant monopole transition strength from the ground state. The transition strength to the  $0_V^+$  state is relatively smaller than those to the lower  $0^+$  states. The present result is consistent with that of the  $4\alpha$ -OCM calculation in Ref. [23]. Detailed discussion of isoscalar monopole excitations is given in the next section.

### C. $E2$ transition strength and band assignment

As mentioned above, the present result suggests the  $^{12}\text{C}(0_2^+)+\alpha$  structure in the  $0_V^+$  state which is regarded as the candidate for the  $4\alpha$  cluster gas state. By analyzing the calculated  $E2$  transition strength, we consider rotational band members from the  $^{12}\text{C}(0_2^+)+\alpha$  structure. The calculated  $E2$  transition strength is shown in Fig.4. The experimental and theoretical  $B(E2)$  values for low-energy states are listed in Table II. For the lowest  $^{12}\text{C}(0_1^+)+\alpha$  cluster band consisting of the  $0_2^+$ ,  $2_1^+$ , and  $4_1^+$  states, the present  $^{12}\text{C}(\text{AMD})+\alpha\text{GCM}$  calculation reproduce reasonably the strong intra-band  $E2$  transitions within a factor two. Twice larger  $B(E2)$  values than the experimental data may suggest  $\sim 20\%$  overestimation of the r.m.s. radii of these states which may come from the higher energy position relative to the  $^{12}\text{C}(0_1^+)+\alpha$  threshold. For the second  $2^+$  state ( $2_{II}^+$ ), which can be understood as the rotational member of the  $0_{III}^+$ , the strong  $E2$  transition to the ground state is inconsistent with the experimental data. This results suggest again that the  $0_{III}^+$  and  $2_{II}^+$  states should be assigned to higher  $0^+$  and  $2^+$  states instead of the  $0_3^+$  and  $2_2^+$  states. If we assign the third and the fourth  $2^+$  states ( $2_{III}^+$  and  $2_{IV}^+$ ) obtained in the present calculation to the  $2_2^+$  and  $2_3^+$  states, the calculated  $B(E2)$  values are in reasonable agreement with the experimental ones.

In the energy region around  $E_x \sim 20$  MeV, we find  $2^+$  states and  $4^+$  states having rather strong (sequential)  $E2$  transition strength toward the  $0_V$  state. In this energy region, there are several  $2^+$  and  $4^+$  states having non-negligible component of the  $^{12}\text{C}(0_2^+)+\alpha$  structure. We also obtain another  $0^+$  state with some  $^{12}\text{C}(0_2^+)+\alpha$  component at 20.3 MeV, a few MeV above the  $0_V$  state. In Fig. 4, the energy levels of these states are shown by solid lines.  $E2$  transition strength is fragmented among them as shown in the figure.

Figure 5 shows the overlap of those states with the  $^{12}\text{C}(0_2^+)+\alpha$  wave function as function of the inter-cluster distance  $d$ . The  $0_V^+$  state has more than 60%  $^{12}\text{C}(0_2^+)+\alpha$  component at  $d_\alpha = 4 - 5$  fm. As the spin increases, the  $^{12}\text{C}(0_2^+)+\alpha$  component decreases and seems scattered into several  $2^+$  and  $4^+$  states. It may imply that the structure change, in other words, the state mixing occurs in the rotation of the  $^{12}\text{C}(0_2^+)+\alpha$  structure.

We also show in Fig. 6 the overlap with the  $^{12}\text{C}(0_1^+)+\alpha$  wave function in the member states of the rotational bands starting from the  $0_{II}^+$  and  $0_{III}^+$  states. As seen in the figure, the lower band build on the  $0_{II}^+$  has the

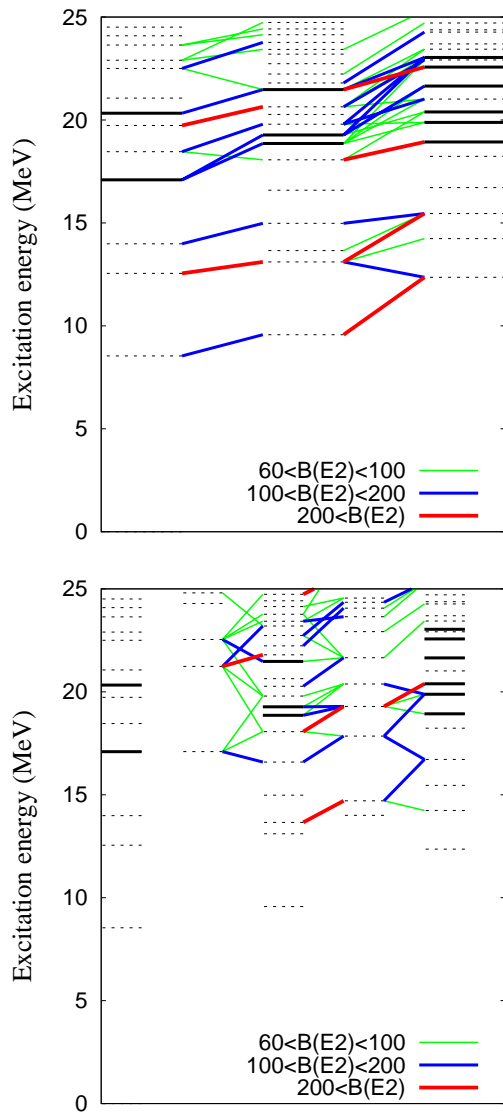


FIG. 4: (Color online) Calculated  $E2$  transition strength in  $^{16}\text{O}$  obtained with the  $^{12}\text{C}(\text{AMD})+\alpha\text{GCM}$ . States having strong  $E2$  transition with  $60 < B(E2) < 100 \text{ e}^2\text{fm}^4$ ,  $100 < B(E2) < 200 \text{ e}^2\text{fm}^4$ , and  $200 < B(E2) \text{ e}^2\text{fm}^4$  are connected by green, blue, and red lines, respectively. (Upper)  $J^\pi = 0^+, 2^+, 4^+$  spectra (dashed) and  $4^+ \rightarrow 2^+$  and  $2^+ \rightarrow 0^+$  transitions (red, blue, and green lines). (Lower)  $J^\pi = 0^+, 1^+, 2^+, 3^+, 4^+$  spectra and  $J^+ \rightarrow (J-1)^+$  transitions. The solid lines are energy levels having significant  $^{12}\text{C}(0_2^+)+\alpha$  component.

$^{12}\text{C}(0_1^+)+\alpha$  structure and higher band from the  $0_{III}^+$  shows the higher nodal feature of the  $^{12}\text{C}(0_1^+)+\alpha$  structure. The overlap with the  $^{12}\text{C}(0_1^+)+\alpha$  wave function in these states does not depend so much on the spin and it is still significant even in the  $4^+$  states.

Thus, the situation is quite different between the  $^{12}\text{C}(0_1^+)+\alpha$  cluster bands and the  $^{12}\text{C}(0_2^+)+\alpha$  bands. The instability of the  $^{12}\text{C}(0_2^+)+\alpha$  states in the rotation is not surprising because the  $^{12}\text{C}(0_2^+)$  cluster is considered

TABLE II:  $E2$  transition strength in  $^{16}\text{O}$ .  $B(E2)$  values calculated with the present  $^{12}\text{C}(\text{AMD})+\alpha\text{GCM}$  and those with the  $^{12}\text{C}+\alpha\text{-OCM}$ [18]. Experimental data are taken from Ref. [34].

initial	final	$B(E2)$ ( $\text{e}^2\text{fm}^4$ )	
		exp.	Ref. [18]
$2^+(6.92)$	$0^+(0)$	$7.4\pm 0.2$	2.48
$2^+(6.92)$	$0^+(6.05)$	$65\pm 7$	60.1
$2^+(9.84)$	$0^+(0)$	$0.07\pm 0.007$	0.489
$2^+(9.84)$	$0^+(6.05)$	$2.9\pm 0.7$	4.64
$2^+(11.5)$	$0^+(0)$	$3.6\pm 1.2$	1.43
$2^+(11.5)$	$0^+(6.05)$	$7.4\pm 1.2$	1.38
$4^+(10.4)$	$2^+(6.92)$	$156\pm 14$	96.2
present			
$2^+_I$	$0^+_I$	3.2	
$2^+_I$	$0^+_{II}$	177	
$2^+_{II}$	$0^+_I$	45	
$2^+_{II}$	$0^+_{II}$	2.3	
$2^+_{III}$	$0^+_I$	0.08	
$2^+_{III}$	$0^+_{II}$	1.4	
$2^+_{IV}$	$0^+_I$	3.1	
$2^+_{IV}$	$0^+_{II}$	0.1	
$4^+_I$	$2^+_I$	290	

to be the  $3\alpha$  cluster gas and such a gas state should not be a rigid but fragile one differently from the  $^{12}\text{C}(0^+_1)$  cluster.

Consequently, it is difficult to clearly identify the band members of the  $^{12}\text{C}(0^+_2)+\alpha$  cluster state, however, considering the relatively strong  $E2$  transition strength and similarity of the  $d$ -dependence of the  $^{12}\text{C}(0^+_2)+\alpha$  overlap, we propose a possible assignment that the  $2^+$  state at 19.3 MeV and  $4^+$  at 21.6 MeV can be regarded as the band members from the  $0^+_2$  state, and the  $2^+$  state at 21.5 MeV and  $4^+$  at 23.0 MeV are interpreted as members of the band starting from the  $0^+_1$  state. Reflecting the structure change, the slope of the energy for  $J(J+1)$  does not show the linear dependence but it becomes gentle with the increase of spin. We also show in Fig. 7 the experimental energy levels of the excited states observed in the  $^{12}\text{C}(^{12}\text{C}, ^8\text{Be}+^8\text{Be})$  and the  $^{12}\text{C}(^{16}\text{O}, 4\alpha)$  reactions[38, 39], which are considered to be candidates for the  $^{12}\text{C}(0^+_2)+\alpha$  cluster states [16]. The calculated energies of the  $^{12}\text{C}(0^+_2)+\alpha$  states measured from the  $^{12}\text{C}(0^+_2)+\alpha$  threshold in the present result qualitatively agree with those of the experimental data.

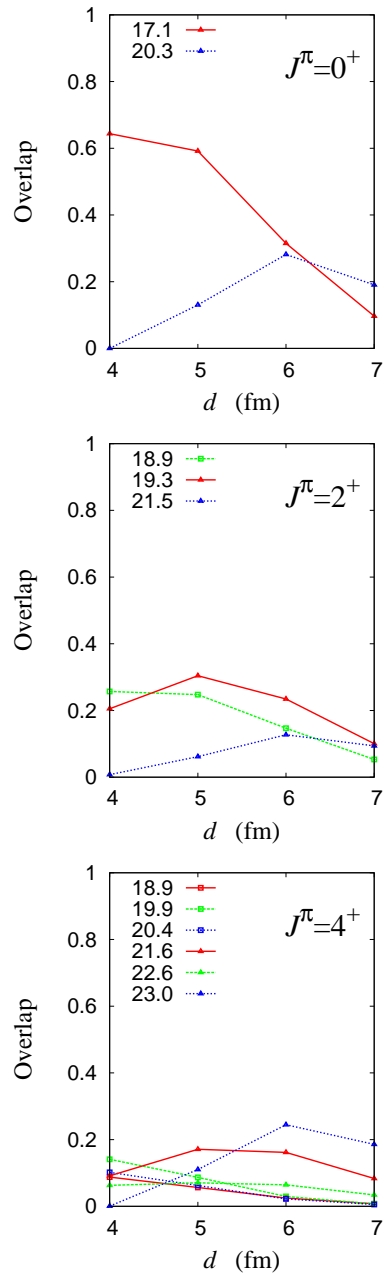


FIG. 5: (Color online) The overlap of the excited  $^{16}\text{O}$  states with the  $^{12}\text{C}(0^+_2)+\alpha$  wave function as a function of the inter-cluster distance  $d$  defined in Eq. 9. The calculated overlap for the  $0^+$  states at 17.1 and 20.3 MeV,  $2^+$  states at 18.9, 19.3, and 21.5 MeV, and  $4^+$  states at 18.9, 19.9, 20.4, 21.6, 22.6 and 23.0 MeV, which have significant  $^{12}\text{C}(0^+_2)+\alpha$  component, is shown.

#### IV. ISOSCALAR MONOPOLE EXCITATION

As discussed recently, isoscalar monopole (ISM) excitation in the low-energy part gives important information on cluster structures of excited states in light nuclei[23, 40]. As well known, the isoscalar giant monopole resonances (ISGMR) in heavy nuclei have been observed as

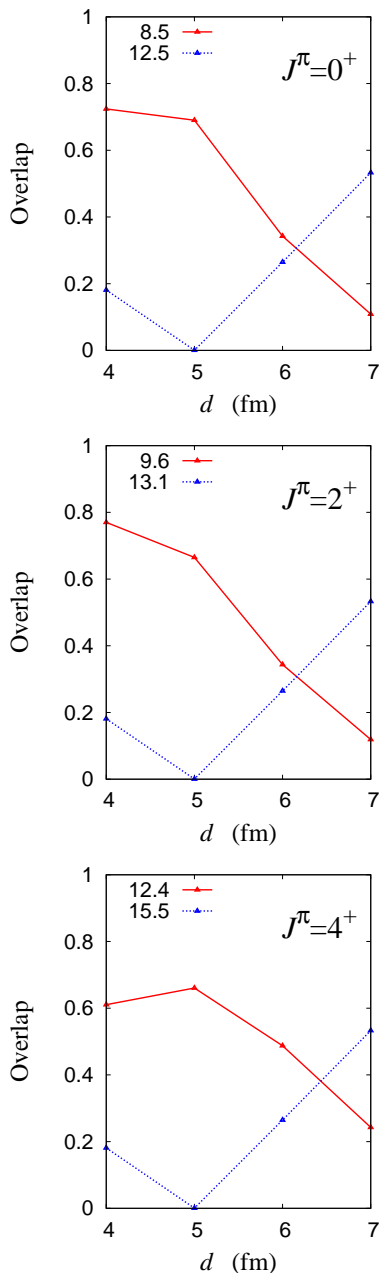


FIG. 6: (Color online) The overlap of the  $^{16}\text{O}$  states with the  $^{12}\text{C}(0_1^+)+\alpha$  wave function as a function of the inter-cluster distance  $d$  defined in Eq. 9. The overlap for the  $0_{II}^+$  at 8.5 MeV,  $2^+$  at 9.6 MeV, and  $4^+$  at 12.4 MeV in the  $^{12}\text{C}(0_1^+)+\alpha$  band, and the  $0_{III}^+$  at 12.5 MeV,  $2^+$  at 13.1 MeV and  $4^+$  at 15.5 MeV in the higher nodal  $^{12}\text{C}(0_1^+)+\alpha$  band is shown.

a single peak and described by the collective breathing mode. The systematics of the peak position has been discussed in association with the nuclear compressibility. In light nuclei such as  $^{12}\text{C}$  and  $^{16}\text{O}$ , however, it has been revealed by the  $(e, e')$  and  $(\alpha, \alpha')$  scattering experiments [41, 42] that the ISM strength is strongly fragmented and significant fraction of the energy-weighted sum rule concentrates on a few states in a low-energy region. Re-

cently, Yamada *et al.* discussed the ISM excitation in  $^{16}\text{O}$  and showed that the significant ISM strength at the low-energy part up to  $E_x \sim 16$  MeV can be described well by the monopole excitation to the cluster states[23]. It was argued that two different types of monopole excitation exist in  $^{16}\text{O}$ , that is, the monopole excitation to cluster states dominating the strength in the lower-energy part and that of the mean-field type  $1p-1h$  excitation yielding the strength in the higher-energy part  $16 \leq E_x \leq 40$  MeV.

In principle, these two modes are not decoupled from but should couple to each other because the cluster excitation partially involves the  $1p-1h$  excitation. Indeed, the ISGMR peak position can be approximately described by the breathing mode of the radial motion of four  $\alpha$  clusters [43]. Therefore, it is expected that the low-lying cluster states feed the strength of a part of the ISGMR strength originally concentrating at the higher energy region.

Although the cluster model calculations such as the 4 $\alpha$ -OCM are useful to describe the cluster excitation, they are not enough to describe the mean-field type  $1p-1h$  excitation because frozen 4  $\alpha$  clusters are assumed. Also the present calculation of the  $^{12}\text{C}(\text{AMD})+\alpha$  may not be sufficient for the  $1p-1h$  excitation because an  $\alpha$  cluster around  $^{12}\text{C}$  is assumed in the model though twelve nucleon dynamics is incorporated in the wave function of the  $^{12}\text{C}$  AMD wave functions. Instead of cluster model calculations, mean-field calculations including particle-hole excitations such as the random phase approximation (RPA) have been applied to investigate ISGMR. In the RPA calculations for  $^{16}\text{O}$  [44–47], it was found that monopole strength spreads out and has a multi peak structure with the centroid around  $E_x = 20 \sim 25$  MeV. They describe the experimental strength in the high-energy region  $E_x \geq 16$  MeV measured by  $(\alpha, \alpha')$  scattering. However, the peak structure with the significant fraction of EWSR in the low-energy part are not reproduced by the mean-field calculations.

To take into account the coexistence of cluster and mean-field features in the ISM excitation, we extend our present framework of the  $^{12}\text{C}(\text{AMD})+\alpha\text{GCM}$  by adding the  $1p-1h$  type basis wave function on the top of the approximate ground state wave function obtained by the  $^{16}\text{O}(\text{AMD}+\text{VAP})$  calculation. After explaining the additional basis wave functions, we discuss the monopole transition in  $^{16}\text{O}$ .

#### A. AMD+VAP calculation of $^{16}\text{O}$ and $1p-1h$ excitation

The present method of the  $^{12}\text{C}(\text{AMD})+\alpha\text{GCM}$  is suitable mainly to describe various types of cluster excitation. To take into account the  $1p-1h$  excitation, we perform the AMD+VAP calculation for  $^{16}\text{O}$  and consider small variations of single-particle wave functions from the obtained ground state wave function. In a similar way to Eq. 1 for  $^{12}\text{C}$ , an AMD wave function for  $^{16}\text{O}$  is written

by a Slater determinant of 16 single-nucleon Gaussian wave packets,

$$\Phi_{16\text{O}}^{\text{AMD}}(\mathbf{Z}) = \frac{1}{\sqrt{A!}} \mathcal{A}\{\varphi_1, \varphi_2, \dots, \varphi_A\}. \quad (11)$$

In the AMD+VAP method, the energy variation is done with respect to the spin-parity eigen wave function  $P_{MK}^{J\pi} \Phi_{16\text{O}}^{\text{AMD}}(\mathbf{Z})$ . After the AMD+VAP calculation for  $^{16}\text{O}$ , we get the optimum AMD solution  $\Phi_{16\text{O}}^{\text{AMD}}(\mathbf{Z}_0)$  which is approximately regarded as the intrinsic wave function of the ground state. Here  $\mathbf{Z}_0$  indicates the set of optimized parameters  $\mathbf{Z}_0 = \{\mathbf{X}_1^0, \mathbf{X}_2^0, \dots, \mathbf{X}_A^0, \xi_1, \dots, \xi_A\}$ .

Then, we vary the spatial part of each single-particle wave function from the AMD wave function,  $\Phi_{16\text{O}}^{\text{AMD}}(\mathbf{Z}_0)$ , by shifting a Gaussian center of the  $i$ th single-particle wave function,  $\mathbf{X}_i^0 \rightarrow \mathbf{X}_i^0 + \delta\mathbf{e}_\sigma$  ( $\sigma = 1, 2, 3$ ). ( $\mathbf{e}_1, \mathbf{e}_2$  and  $\mathbf{e}_3$  are the three-dimension unit vectors.) For all single-particle wave function, we consider a small shift to three directions independently, namely,  $A \times 3$  kinds of shifted wave functions  $\Phi_{16\text{O}}^{\text{AMD}}(\mathbf{Z}'_0(i, \sigma))$  ( $i = 1, \dots, A$  and  $\sigma = 1, 2, 3$ ) with  $\mathbf{Z}'_0(i, \sigma) \equiv \{\mathbf{X}_1^0, \dots, \mathbf{X}_i^0 + \delta\mathbf{e}_\sigma, \dots, \mathbf{X}_A^0, \xi_1, \dots, \xi_A\}$ . By using the linear combination of 47 wave functions, the original wave function  $\Phi_{16\text{O}}^{\text{AMD}}(\mathbf{Z}_0)$  and the shifted ones  $\Phi_{16\text{O}}^{\text{AMD}}(\mathbf{Z}'_0(i, \sigma))$ ,  $1p$ - $1h$  excitations in the intrinsic frame are incorporated. We fix the spin orientations  $\xi_i$  and consider the  $1p$ - $1h$  excitations mainly for spatial part. For excited  $0^+$  states of  $^{16}\text{O}$ , we superpose the spin-parity eigen states projected from those wave functions,  $P_{MK}^{J\pi} \Phi_{16\text{O}}^{\text{AMD}}(\mathbf{Z}_0)$  and  $P_{MK}^{J\pi} \Phi_{16\text{O}}^{\text{AMD}}(\mathbf{Z}'_0(i, \sigma))$ . The coefficients of each basis wave functions are determined by diagonalizing the norm and Hamiltonian matrices. We call this calculation " $^{16}\text{O}(\text{AMD})+1p$ - $1h$ ".

In addition to the  $^{16}\text{O}(\text{AMD})+1p$ - $1h$  calculation in the  $1p$ - $1h$  model space, we also perform the hybrid calculation of  $^{12}\text{C}(\text{AMD})+\alpha\text{GCM}$  and  $^{16}\text{O}(\text{AMD})+1p$ - $1h$  by superposing all basis wave functions. The coefficients are determined again by the diagonalization.

## B. Monopole transitions

The strength function of the ISM excitation from the ground state of  $^{16}\text{O}$  is

$$S(E) \equiv \delta(E - E_n) |M(\text{IS0}, 0_1^+ \rightarrow 0_n^+)|^2 \quad (12)$$

$$M(\text{IS0}, 0_1^+ \rightarrow 0_n^+) = \langle 0_n^+ | \sum_{i=1}^{16} \mathbf{r}_i^2 | 0_1^+ \rangle. \quad (13)$$

For the isoscalar excitation, this is 4 times as much as the isoscalar  $E0$  strength function defined in Refs. [41, 42]. The EWSR of the ISM transition is

$$\sum_n (E_n - E_1) |M(\text{IS0}, 0_1^+ \rightarrow 0_n^+)|^2 = \frac{2\hbar^2}{m} 16 \langle r^2 \rangle, \quad (14)$$

where  $\langle r^2 \rangle$  is the mean square matter radius of the ground state,

$$\langle r^2 \rangle = \frac{1}{16} \langle 0_1^+ | \sum_{i=1}^{16} \mathbf{r}_i^2 | 0_1^+ \rangle. \quad (15)$$

In the results of the  $^{12}\text{C}(\text{AMD})+\alpha\text{GCM}$ , the  $^{16}\text{O}(\text{AMD})+1p$ - $1h$ , and the hybrid of  $^{12}\text{C}(\text{AMD})+\alpha\text{GCM}$  and  $^{16}\text{O}(\text{AMD})+1p$ - $1h$ , the energy weighted sum of the ISM strength for all excited states is 93%, 87%, and 95% of the EWSR value, and that for excited states up to 40 MeV ( $E_x \leq 40$  MeV) is 77%, 64%, 69%, respectively.

In the present calculation, all excited states are discrete states because of the bound state approximation. We calculate the ISM transition matrix element  $M(\text{IS0})$  for  $0_n^+$  states of the  $^{12}\text{C}(\text{AMD})+\alpha\text{GCM}$ , the  $^{16}\text{O}(\text{AMD})+1p$ - $1h$ , and the hybrid full calculations. The calculated ISM transition strength ( $B(\text{IS0}) = |M(\text{IS0})|^2$ ) is shown in the histogram in Fig. 8, where the strength  $|M(\text{IS0})|^2$  for  $0_n^+$  states in each energy bin is summed up.

In the  $^{12}\text{C}(\text{AMD})+\alpha\text{GCM}$  result, the significant strength exists in the low-energy part for the  $0_{II}^+$ ,  $0_{III}^+$ , and  $0_{IV}^+$  states having the  $^{12}\text{C}(0_1^+, 2_1^+)+\alpha$  cluster structures. They exhaust  $\sim 30\%$  of the EWSR. Such the large fraction in the low-energy part ( $E_x \leq 16$  MeV) is comparable to the  $4\alpha$ -OCM calculation where  $\sim 20\%$  of the EWSR exists in the  $E_x \leq 16$  MeV part [23]. In higher-energy region, the strength concentrates around the region  $E_x \sim 20$  MeV. The EWSR ratio of the high-energy part ( $16 \leq E_x \leq 40$  MeV) is  $\sim 45\%$  in the  $^{12}\text{C}(\text{AMD})+\alpha\text{GCM}$  calculation.

In the result of the  $^{16}\text{O}(\text{AMD})+1p$ - $1h$  calculation, the ISM transition strength shows the two-peak structure around  $E_x \sim 20$  MeV, one below and the other above  $E_x = 20$  MeV. The higher peak corresponds to the breathing mode which can be described by the coherent isotropic single-particle motion, while the lower peak is understood as the motion of one  $\alpha$ -cluster against the  $^{12}\text{C}$  core. The latter mode originates in the ground state  $\alpha$  correlation around the  $^{12}\text{C}$  core which is contained in the AMD+VAP result of  $^{16}\text{O}(0_1^+)$ . The lower and the higher peaks exhaust about 20% and 40% of the EWSR, respectively. The EWSR ratio for the lower peak is the same order of the EWSR ratio for the cluster states with the  $^{12}\text{C}(0_1^+, 2_1^+)+\alpha$  cluster structures in  $E_x \leq 16$  MeV calculated with the  $^{12}\text{C}(\text{AMD})+\alpha\text{GCM}$ .

The full calculation using the hybrid model space of the  $^{12}\text{C}(\text{AMD})+\alpha\text{GCM}$  and the  $^{16}\text{O}(\text{AMD})+1p$ - $1h$  shows qualitatively similar features of the  $^{12}\text{C}(\text{AMD})+\alpha\text{GCM}$  calculation. Namely, there exist three peaks corresponding to the cluster states in the low-energy part ( $E_x \leq 16$  MeV), and the concentration of the strength around the peak-like structure slightly above 20 MeV. The EWSR ratios of the low-energy part ( $E_x \leq 16$  MeV) and the high-energy part ( $16 \leq E_x \leq 40$  MeV) are  $\sim 25\%$  and  $\sim 40\%$ , respectively.

Comparing the results of the  $^{12}\text{C}(\text{AMD})+\alpha\text{GCM}$ , the

$^{16}\text{O}+(1p-1h)$ , and the full hybrid calculations, it is found that there is no significant difference of the EWSR ratios of the low-energy and high-energy parts among three calculations. It implies that two modes around  $\sim 20$  MeV obtained in the  $^{16}\text{O}(\text{AMD})+1p-1h$  are involved in excited states of the  $^{12}\text{C}(\text{AMD})+\alpha\text{GCM}$ . That is, the higher peak of the collective breathing mode corresponds to the peak-like structure slightly above 20 MeV in the  $^{12}\text{C}(\text{AMD})+\alpha\text{GCM}$  and the full calculation, while the lower mode for the  $^{12}\text{C}-\alpha$  motion is fragmented in the lowest three excited  $0^+$  states with the  $^{12}\text{C}(0_1^+, 2_1^+)+\alpha$  cluster structures. Namely, we can conclude the origins of isoscalar monopole excitations as follows. In the mean-field type  $1p-1h$  excitation there exist two modes around  $E_x \sim 20$  MeV. The lower mode corresponds to the  $^{12}\text{C}-\alpha$  relative motion and the higher one is the collective breathing mode. Because of the coupling with the cluster excitation, the lower mode is fragmented into several cluster states in  $E_x \leq 16$  MeV while lowering the energy centroid. The strength of the higher breathing mode is somehow spread and also its energy centroid is lowered to contribute to the strength around  $E_x \sim 20$  MeV.

The ISM transition strength has been observed by  $(\alpha, \alpha')$  scattering [42]. The measured strength for the  $0^+$  states at 12 and 14 MeV is smaller than the that observed by  $(e, e')$  scattering by a factor 2–4. Moreover, their measurement in the energy region  $11 < E_x < 40$  MeV yields only  $\sim 50\%$  of the  $E0$  EWSR. These fact may suggest possible ambiguity of the normalization in the ISM strength measured by  $(\alpha, \alpha')$  scattering. We multiply the experimental data by a factor 2 and show the values in Fig. 8(d) to compare the shape of strength function with our result. Comparing the result of the full calculation with the experimental data, it is shown that the strength for the  $0_{III}^+$  and  $0_{IV}^+$  states at 13 and 15 MeV may describe the peaks in the  $11 < E_x < 16$  MeV of the experimental data. The significant strength in the higher region around 20 MeV is considered to correspond to the bump structures in the regions  $16 < E_x < 20$  MeV and/or  $20 < E_x < 25$  MeV. The calculated strength are not fragmented so much as the experimentally measured one, maybe, because of the limitation of the present model space. The EWSR ratio of the full calculation and that of the experimental data are shown in Fig. 9. We again multiply the experimental data of Ref. [42] measured by  $(\alpha, \alpha')$  scattering by a factor 2 in the plotting.

## V. SUMMARY AND OUTLOOKS

Cluster structures and monopole transitions in positive parity states of  $^{16}\text{O}$  were investigated based on the  $^{12}\text{C}(\text{AMD})+\alpha\text{GCM}$  calculation. The lowest three excited  $0^+$  states ( $0_{II}^+$ ,  $0_{III}^+$ , and  $0_{IV}^+$ ) have the  $^{12}\text{C}(0_1^+, 2_1^+)+\alpha$  cluster structures. The  $0_{II}^+$  with the  $^{12}\text{C}(0_1^+)+\alpha$  structure and its rotational band members qualitatively reproduce the properties such as energy levels and  $E2$  and monopole transition strengths for the

experimental  $0_2^+$ ,  $2_1^+$ , and  $4_1^+$  states, which have been considered to be the  $^{12}\text{C}(0_1^+)+\alpha$  cluster band. As far as we know, the present calculation is the first microscopic calculation that can describe reasonably the excitation energies of these excited states.

In the present calculation, we obtained the fifth  $0^+$  state ( $0_V^+$ ) having the developed  $^{12}\text{C}(0_2^+)+\alpha$  structure. Because of the feature that an  $\alpha$  cluster is moving in the  $L = 0$  wave around the  $^{12}\text{C}(0_2^+)$ , it is regarded as the  $4\alpha$  cluster gas state similar to the  $3\alpha$  cluster gas in the  $^{12}\text{C}(0_2^+)$ . This state may correspond to the  $0_6^+$  state of the  $4\alpha$  cluster gas state suggested in the  $4\alpha\text{-OCM}$  by Funaki *et al.* [5, 6].

With the analyses of the  $E2$  transition strength and the  $^{12}\text{C}(0_2^+)+\alpha$  component, we considered band members of the  $^{12}\text{C}(0_2^+)+\alpha$  cluster state. Around  $E_x \sim 20$  MeV, there are several  $2^+$  and  $4^+$  states having some component of  $^{12}\text{C}(0_2^+)+\alpha$ . The  $E2$  transition strength is fragmented among them. The present result suggests that the structure change, in other words, the state mixing occurs in the rotation of the  $^{12}\text{C}(0_2^+)+\alpha$  cluster structure. It make it difficult to assign clearly the  $^{12}\text{C}(0_2^+)+\alpha$  band members in high spin states. This feature is different from that of the  $^{12}\text{C}(0_1^+)+\alpha$  cluster band and may originate in the  $3\alpha$  cluster gas feature of the  $^{12}\text{C}(0_2^+)$  that might be fragile in the rotation.

The isoscalar monopole excitation was discussed with the  $^{12}\text{C}(\text{AMD})+\alpha\text{GCM}$  and also with the hybrid calculation of the  $^{12}\text{C}(\text{AMD})+\alpha\text{GCM}$  and  $^{16}\text{O}(\text{AMD})+1p-1h$ . In the strength of both calculations, there exist three peaks for the cluster states in the low-energy part ( $E_x < 16$  MeV). This is consistent with the preceding work with the  $4\alpha\text{-OCM}$  calculation [23]. We also found the concentration of the strength around the peak-like structure slightly above  $E_x \sim 20$  MeV, which originates in the collective breathing mode. Comparing the hybrid calculation with the  $^{16}\text{O}+1p-1h$  calculation, we conclude the origins of isoscalar monopole excitations as follows. In the mean-field type  $1p-1h$  excitation there exist two modes around  $E_x = 20$  MeV. The lower mode corresponds to the  $^{12}\text{C}-\alpha$  relative motion and the higher one is the collective breathing mode. Because of the coupling with the cluster excitation, the lower mode is fragmented into several cluster states in  $E_x < 16$  MeV while lowering the energy centroid. The higher-energy breathing mode is somehow spread and its energy centroid is lowered to contribute to the strength around  $E_x \sim 20$  MeV.

The present calculation is a bound state approximation. The stability of the excited states should be studied in more details by taking into account coupling with continuum states. We also should reexamine the choice of the effective interaction and the interaction parameters for quantitative reproduction of energy levels. In the present work, we used the same phenomenological effective nuclear forces as those used in the previous work on  $^{12}\text{C}$ . The energy spectra of  $^{16}\text{O}$  may be improved by fine tuning of the interaction parameters. However, we have some difficulty in completely reproducing the bind-

ing energies of  $\alpha$ ,  $^{12}\text{C}$ , and  $^{16}\text{O}$  as well as the energy spectra of the subsystem  $^{12}\text{C}$  simultaneously with such the phenomenological effective nuclear interaction. *Ab initio* calculation based on realistic nuclear force is one of the promising tools for quantitative prediction of energy spectra of  $^{16}\text{O}$  though applications of *ab initio* calculations to cluster states are still limited.

### Acknowledgments

The author would like to thank Dr. Funaki and Dr. Yamada for fruitful discussions. The computational calcu-

lations of this work were performed by using the supercomputers at YITP. This work was supported by Grant-in-Aid for Scientific Research from Japan Society for the Promotion of Science (JSPS). It was also supported by the Grant-in-Aid for the Global COE Program "The Next Generation of Physics, Spun from Universality and Emergence" from the Ministry of Education, Culture, Sports, Science and Technology (MEXT) of Japan.

- 
- [1] A. Tohsaki, H. Horiuchi, P. Schuck and G. Ropke, Phys. Rev. Lett. **87**, 192501 (2001).
- [2] Y. Funaki, H. Horiuchi, A. Tohsaki, P. Schuck and G. Ropke, Prog. Theor. Phys. **108**, 297 (2002).
- [3] T. Yamada and P. Schuck, Phys. Rev. C **69**, 024309 (2004).
- [4] Y. Funaki, A. Tohsaki, H. Horiuchi, P. Schuck and G. Ropke, Phys. Rev. C **67**, 051306 (2003).
- [5] Y. Funaki, T. Yamada, H. Horiuchi, G. Ropke, P. Schuck and A. Tohsaki, Phys. Rev. Lett. **101**, 082502 (2008).
- [6] Y. Funaki, T. Yamada, A. Tohsaki, H. Horiuchi, G. Ropke and P. Schuck, Phys. Rev. C **82**, 024312 (2010).
- [7] T. Yamada, Y. Funaki, H. Horiuchi, G. Ropke, P. Schuck and A. Tohsaki, Lect. Notes Phys. **848**, 229 (2012).
- [8] Y. Kanada-En'yo, Phys. Rev. C **75**, 024302 (2007).
- [9] Y. Kanada-En'yo, Phys. Rev. C **76**, 044323 (2007).
- [10] N. Itagaki, M. Kimura, C. Kurokawa, M. Ito and W. von Oertzen, Phys. Rev. C **75**, 037303 (2007).
- [11] T. Suhara and Y. Kanada-En'yo, Phys. Rev. C **85**, 054320 (2012).
- [12] T. Ichikawa, N. Itagaki, Y. Kanada-En'yo, T. Kokalova and W. von Oertzen, Phys. Rev. C **86**, 031303 (2012).
- [13] F. Kobayashi and Y. Kanada-En'yo, Phys. Rev. C **86**, 064303 (2012).
- [14] F. Kobayashi and Y. Kanada-En'yo, arXiv:1305.4323 [nucl-th].
- [15] T. Wakasa, E. Ihara, K. Fujita, Y. Funaki, K. Hatanaka, H. Horiuchi, M. Itoh and J. Kamiya *et al.*, Phys. Lett. B **653**, 173 (2007).
- [16] S. Ohkubo, Y. Hirabayashi and Y. Hirabayashi, Phys. Lett. B **684**, 127 (2010).
- [17] Y. Funaki, T. Yamada, H. Horiuchi, G. Ropke, P. Schuck and A. Tohsaki, Prog. Theor. Phys. Suppl. **196**, 439 (2012).
- [18] Y. Suzuki, Prog. Theor. Phys. **55**, 1751 (1976); **56**, 111 (1976).
- [19] M. Libert-Heinemann, D. Baye, and P.-H. Heenen, Nucl. Phys. A **339**, 429 (1980).
- [20] K. Ikeda, H. Horiuchi, and S. Saito, Prog. Theor. Phys. Suppl. **68**, 1 (1980).
- [21] S. Saito, Prog. Theor. Phys. **40**, 893 (1968); **41**, 705 (1969); Prog. Theor. Phys. Suppl. **62**, 11 (1977).
- [22] K. Fukatsu and K. Katō, Prog. Theor. Phys. **87**, 151 (1992).
- [23] T. Yamada, Y. Funaki, T. Myo, H. Horiuchi, K. Ikeda, G. Ropke, P. Schuck and A. Tohsaki, Phys. Rev. C **85**, 034315 (2012).
- [24] J. A. Wheeler, Phys. Rev. **32**, 1083 (1937).
- [25] D. L. Hill and J. A. Wheeler, Phys. Rev. **89**, 1102 (1953); J. J. Griffin and J. A. Wheeler, Phys. Rev. **108**, 311 (1957).
- [26] Y. Kanada-En'yo, H. Horiuchi and A. Ono, Phys. Rev. C **52**, 628 (1995); Y. Kanada-En'yo and H. Horiuchi, Phys. Rev. C **52**, 647 (1995).
- [27] Y. Kanada-En'yo and H. Horiuchi, Prog. Theor. Phys. Suppl. **142**, 205 (2001); Y. Kanada-En'yo M. Kimura and H. Horiuchi, C. R. Physique **4**, 497 (2003); Y. Kanada-En'yo, M. Kimura and A. Ono, PTEP **2012** (2012) 01A202.
- [28] Y. Kanada-En'yo, Phys. Rev. Lett. **81**, 5291 (1998).
- [29] Y. Kanada-En'yo, Prog. Theor. Phys. **117**, 655 (2007) [Erratum-ibid. **121**, 895 (2009)].
- [30] T. Ando, K. Ikeda and A. Tohsaki, Prog. Theory. Phys. **64**, 1608 (1980).
- [31] K. Minomo, T. Sumi, M. Kimura, K. Ogata, Y. R. Shimizu and M. Yahiro, Phys. Rev. Lett. **108**, 052503 (2012).
- [32] Y. Kanada-En'yo, Phys. Rev. C **85**, 044320 (2012).
- [33] N. Yamaguchi, T. Kasahara, S. Nagata and Y. Akaishi, Prog. Theor. Phys. **62**, 1018 (1979); R. Tamagaki, Prog. Theor. Phys. **39**, 91 (1968).
- [34] D. R. Tilley, H. R. Weller and C. M. Cheves, Nucl. Phys. A **564**, 1 (1993).
- [35] I. Angeli, At. Data Nucl. Data Tables **87**, 185 (2004).
- [36] F. Ajzenberg-Selove, Nucl. Phys. A **460**, 1 (1986).
- [37] T. Yamada and P. Schuck, Eur. Phys. J. A **26**, 185 (2005).
- [38] P. Chevallier, F. Scheibling, G. Goldring, I. Plesser and M. W. Sachs, Phys. Rev. **160**, 827 (1967).
- [39] M. Freer, N. M. Clarke, N. Curtis, B. R. Fulton, S. J. Hall, M. J. Leddy, J. S. Pople and G. Tungate *et al.*, Phys. Rev. C **51**, 1682 (1995).
- [40] T. Yamada, Y. Funaki, H. Horiuchi, K. Ikeda, and A. Tohsaki, Prog. Theor. Phys. **120**, 1139 (2008).
- [41] M. W. Krison, Nucl. Phys. A **257**, 58 (1976).
- [42] Y. -W. Lui, H. L. Clark and D. H. Youngblood, Phys. Rev. C **64**, 064308 (2001).
- [43] T. Furuta, K. H. O. Hasnaoui, F. Gulminelli, C. Leclercq and A. Ono, Phys. Rev. C **82**, 034307 (2010).

- [44] J. P. Blaizot, D. Gogny and B. Grammaticos, Nucl. Phys. A **265**, 315 (1976).
- [45] Z. Ma, N. Van Giai, H. Toki and M. L'Huillier, Phys. Rev. C **55**, 2385 (1997).
- [46] P. Papakonstantinou and R. Roth, Phys. Lett. B **671**, 356 (2009).
- [47] D. Gambacurta, M. Grasso and F. Catara, Phys. Rev. C **81**, 054312 (2010).

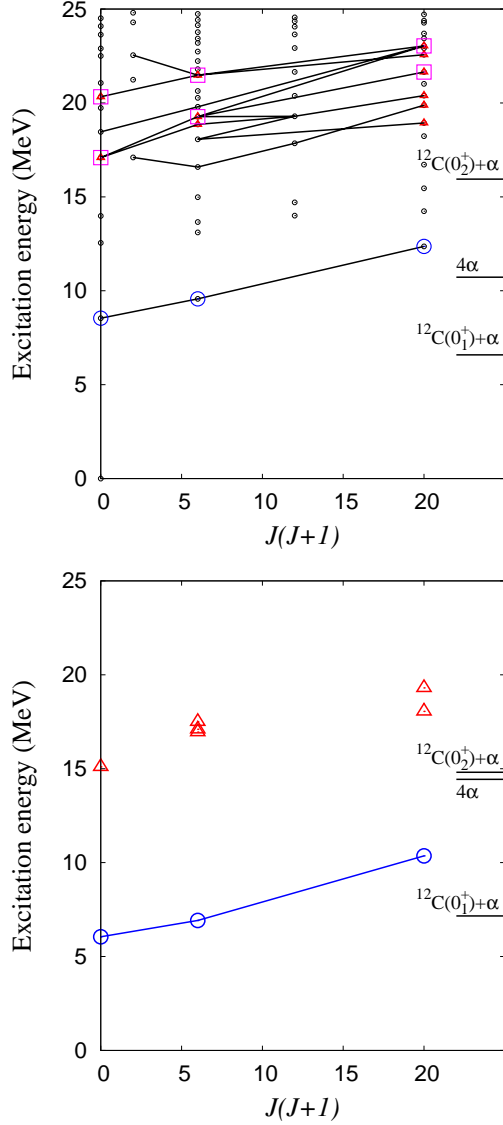


FIG. 7: (Color online) Upper: theoretical excitation levels of  $^{16}\text{O}$  calculated with the  $^{12}\text{C}(\text{AMD})+\alpha\text{GCM}$  (circles). Excited states with significant  $^{12}\text{C}(0_2^+)+\alpha$  component are shown by red triangles and squares. States connected by the lines are those which can be connected to the  $4^+$  states with the  $^{12}\text{C}(0_2^+)+\alpha$  component by the strong (sequential) transitions. Squares indicate possible band assignment for the  $^{12}\text{C}(0_2^+)+\alpha$  cluster states. Circles shows the band members of the  $^{12}\text{C}(0_1^+)+\alpha$  cluster structure starting from the  $0_{II}^+$  state. Lower: experimental excitation energies of the candidate states for the  $^{12}\text{C}(0_2^+)+\alpha$  cluster states observed by the  $^{12}\text{C}(^{12}\text{C}, ^8\text{Be}+^8\text{Be})$  and the  $^{12}\text{C}(^{16}\text{O}, 4\alpha)$  reactions[38, 39], and those of the band members of the  $^{12}\text{C}(0_1^+)+\alpha$  structure[34].

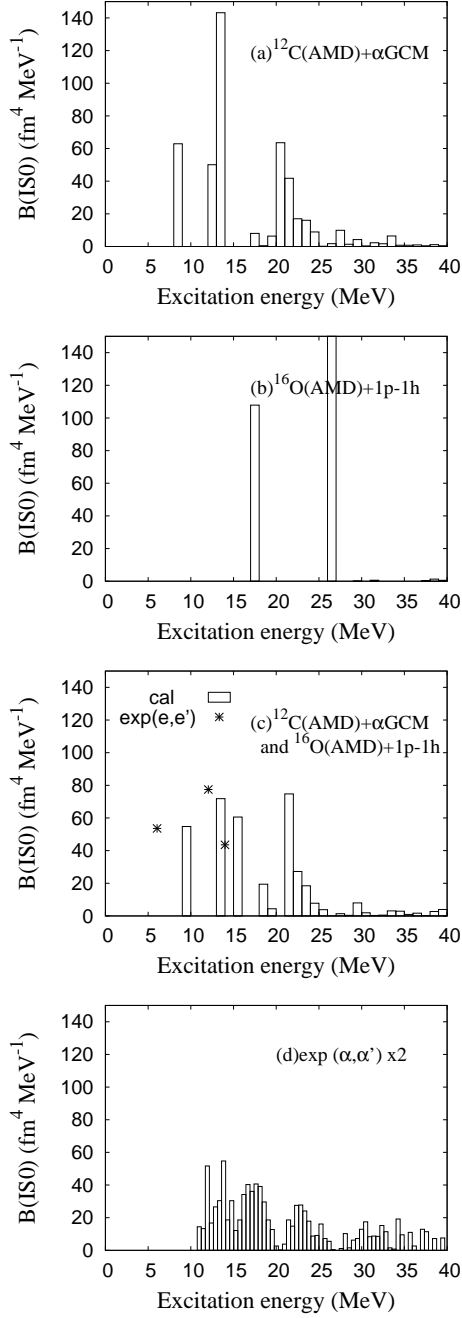


FIG. 8: Isoscalar monopole transition strength function. The theoretical  $B(IS0)$  calculated with (a) the  $^{12}\text{C}(\text{AMD})+\alpha\text{GCM}$ , (b) the  $^{16}\text{O}(\text{AMD})+1p-1h$ , and (c) the hybrid of  $^{12}\text{C}(\text{AMD})+\alpha\text{GCM}$  and  $^{16}\text{O}(\text{AMD})+1p-1h$ . In the histogram the strength in each energy bin is summed up. The experimental  $B(IS0)$  ( $\text{fm}^4$ ) converted from the  $B(E0)$  measured by  $(e, e')$  scattering for the  $0^+$  states at 6.05 MeV, 12.05 MeV, and 14.01 MeV are also shown by stars in the third panel (c). (d) The experimental data measured by  $(\alpha, \alpha')$  scattering. We multiply the data from Ref. [42] by a factor 2 in the panel (d).

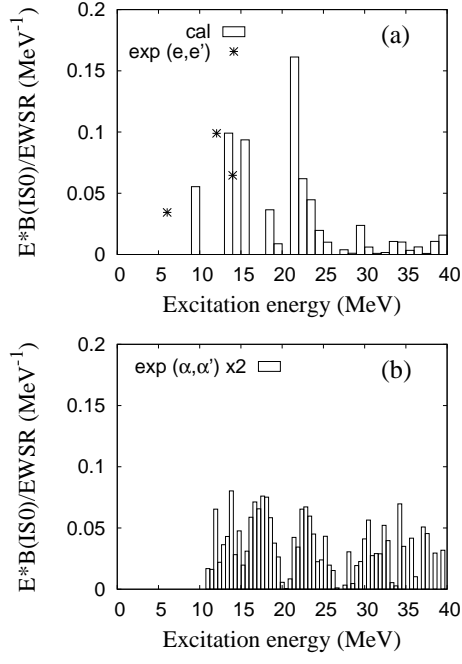


FIG. 9: The ratio of the energy weighted sum to the total EWSR. (a) The theoretical values calculated with the hybrid of  $^{12}\text{C}(\text{AMD})+\alpha\text{GCM}$  and  $^{16}\text{O}(\text{AMD})+1p-1h$ . (b) The experimental data measured by  $(\alpha, \alpha')$  scattering. We multiply the data from Ref. [42] by a factor 2 in the plot.